Simulation-assisted design of a catalytic hydrogenation reactor for plastic pyrolysis fuels

Alberto Gala[a], David Catalán-Martínez[b], Marta Guerrero[a], José Manuel Serra[b,*]

[a] Department of Innovation, Technological Waste Innovation Centre (CIAM), URBASER S.A., C/Azufre, 120, 50720 La Cartuja Baja (Zaragoza), Spain

[b] Instituto de Tecnología Química, Universitat Politècnica de València – Consejo Superior de Investigaciones Científicas, 46022 Valencia, Spain.

* Corresponding author

E-mail address: jmserra@itq.upv.es

Declarations of interest: none

Abstract

An enhancement of the properties of pyrolysis liquids (PL) from municipal plastic waste (mainly low-density polyethylene) by catalytic hydrotreatment is required to obtain automotive quality fuels. In this context, we report the design of a pilot catalytic hydrotreatment reactor using computational fluid dynamics (CFD). This modelling technique considered fluid flows, gas diffusion, olefin hydrogenation reactions, and heat transfer. The built model allowed the development of different sensitive analysis to evaluate the influence of spatial time, heat transfer fluid (used as a reactor coolant) and hydrogen/pyrolysis liquid ratio. Possible phase changes (from gas to liquid) were analyzed by a thermodynamic approach. The results showed that the refrigerant oil allows alleviating possible temperature gradients arising from the exothermic hydrogenation reaction. It was also found that the system can be optimized in order to minimize the

energy cost by adjusting the inlet temperature of the reactive gas (H_2) and the refrigerant oil flow. Condensations in the reactive chamber could be avoided by working at intermediate pressures (40-60 bar) and/or increasing the feed of H_2. Additionally, the results obtained with the CFD 3D model together with the condensation analysis allowed to optimize the operational regime and the pilot-reactor design in terms of dimensioning and construction materials.

Keywords

CFD, hydrotreatment, pyrolysis, LDPE, automotive fuels

1. Introduction

In the last decades, the continuous increment in the consumption of plastic materials has brought about a great rise in the amount of plastic waste. The magnitude of the problem can be estimated considering the worldwide plastic production, which increased from 1.5 Mt in 1950 to 348 Mt in 2017 and it could triple in 2050 [1]. Note that if the current trend continues, 33 billion tons of plastic will be accumulated on the planet [2].

Approximately 70 % of European plastic waste (18.5 Mt/year) is not being recycled due to technical or economic reasons, and thus it is sent to landfill (27 %) or incinerated (42 %) [1]. These circumstances affect the environment negatively in terms of pollution and greenhouse gas emissions, as well as social perception regarding waste management, consumer's product industry, and policy makers [3,4]. Furthermore, this situation is really alarming because plastics are still high-value resources that can be reused or transformed into new feedstock or fuels at the end of their lifetime. Therefore, there is a need to combine mechanical recycling methods with alternative valorization options (i.e. chemical recycling) in order to manage the huge amount of plastic waste [3–5]. The combination of these technologies is emerging as the only way to comply with regulatory objectives (regarding waste disposal) to reduce the quantity of non-recycled plastic waste sent to landfill, and to develop a circular economy strategy [6].

Low-density polyethylene (LDPE) is the second most demanded plastic material worldwide, amounting to approximately 9 Mt in 2017 [1]. In this sense, it is clear the tremendous interest of a process that would allow the conversion of LDPE into a valuable product. One of the most promising options to valorize this kind of plastic waste is the production of fuels (i.e. automotive diesel) by means of a thermochemical process, and pyrolysis seems to be the predominant technology used. As has been reported in the literature [7], the pyrolysis of LPDE allows the conversion of the polymer into a liquid

similar to the diesel coming from petrochemical feedstock [8]. This process involves the thermal decomposition of large polymeric chains into smaller molecules at moderate to high temperatures (400-800 ºC) in the absence of oxygen, thus obtaining very valuable products with high potential to be used as fuels or petrochemical feedstock [7,9,10]. Although the quantity and quality of the products depend on waste plastic composition and the parameters used in the process [10,11], pyrolysis is an appropriate process to maximize the liquid yield, as proved by several studies, which have reached above 75 % yield of liquids by processing polyolefins using catalytic or non-catalytic pyrolysis [12–20]. When LDPE is used as feedstock, pyrolysis liquids result in a product free from oxygenated compounds and with a relatively low heteroatom content. However, other properties (i.e. sulphur content, oxidative stability, density or flash point) prevent its direct use as automotive fuel [21]. Therefore, it is necessary an upgrading catalytic step (i.e. hydrotreatment) to enhance oxidative stability and to reduce sulphur content [22], and a distillation step [23] to reach a density and a flash point that meet the requirements for automotive diesel (class A) established by the EN 590:2014 + A1:2017 standard [24].

As has been reported [22,25], catalytic hydrotreatment looks promising for overcoming the pyrolysis liquid limitations associated with the high content in olefins, as well as to tune the properties of the fuels by choosing suitable catalysts and operation conditions. This process involves the treatment of the pyrolysis liquids with hydrogen in combination with a suitable solid catalyst at elevated temperatures and pressures [26,27], in order to remove sulphur and other impurities, as well as to increase the oxidative stability by decreasing unsaturated hydrocarbons. In hydrogen rich atmosphere, coke formation can be suppressed, and therefore the catalyst lifetime with high catalytic activity can be prolonged [28]. The design of the catalytic unit is very complex because the

hydrotreatment process is a strongly exothermic reaction, demanding a very precise control of temperature. To that end, computational fluid dynamics (CFD) approach [29][30][31] is a very powerful tool to get data from a hypothetical reactor before its construction, providing information about thermofluid-dynamic, heat and mass transfer [32], and thus guaranteeing that the reactor can be successfully designed and optimized to run in a real and in-operation plant. The finite element method or computational fluid dynamics is used to solve physical problems in engineering analysis and design [33]. Finite elements approach allows forward and complete analysis of a setup (for dynamic or steady states) considering the phenomena that take place and the properties of the materials. The methodology is based on a discretization of the geometry in interconnected nodes. The more complex the geometry and/or the process, the higher computational resources are required to carry on. The analysis of an engineering system usually requires the idealization of the system into a form that can be solved, the formulation of the mathematical model, the solution of the model, and the interpretation of the results.

The utilization of finite elements requires a validation step, which allows to demonstrate the model, and offering suitable predictions by comparing with the experimental results. Several studies are focused on the validation steps due to the high number of variables needed to model the process phenomena [34–36]. CFD models are usually used to find the optimal process conditions [37–40], evaluate the scale up, and design the final commercial setup [41].

In this context, the aim of this paper is to design an adequate catalytic reactor to carry out the hydrotreatment of liquids (30 kg/h) coming from LDPE pyrolysis performed in an pilot plant [21], using a heat transfer fluid to ensure the operational temperature and isothermal performance. To accomplish this objective, advanced simulation tools have been used as support. This paper describes the CFD model that has been developed to

optimize and design the pilot catalytic hydrotreatment reactor to carry out the upgrading of the LDPE pyrolysis liquids. The model includes fluid flow, olefin hydrogenation reactions, diffusion of gas species, and heat transfer. A comprehensive sensitive analysis to assess the influence of the main operating parameters has also been performed, including spatial time, heat transfer fluid (used as a reactor coolant), and hydrogen/pyrolysis liquid ratio. Possible phase changes (from gas to liquid) have also been evaluated from a thermodynamic point of view.

2. Materials and Methods

2.1. Urbaser pilot plant and pyrolysis liquid properties

Urbaser company has recently developed a plastic-to-oil (PtO) process to carry out the chemical recycling of polyolefins recovered from municipal solid waste (MSW), obtaining a high-quality liquid product. In general terms, the pyrolysis process (Figure 1a) consists [21] of two clearly differentiated steps: (1) melting the plastic waste, and (2) thermal cracking procedure. During the pyrolysis process, the chains of LDPE, previously melted, crack into smaller pieces of liquid hydrocarbons to obtain a mixture of compounds (mainly paraffins, olefins and aromatics) ranging from 5 (C5) to 32 (C32) carbon atoms (Figures 1b and 1c). The properties analyzed for the pyrolysis liquids and some requirements for automotive diesel, according to the EN 590:2014 + A1:2017 standard [24], are shown in Table 1.

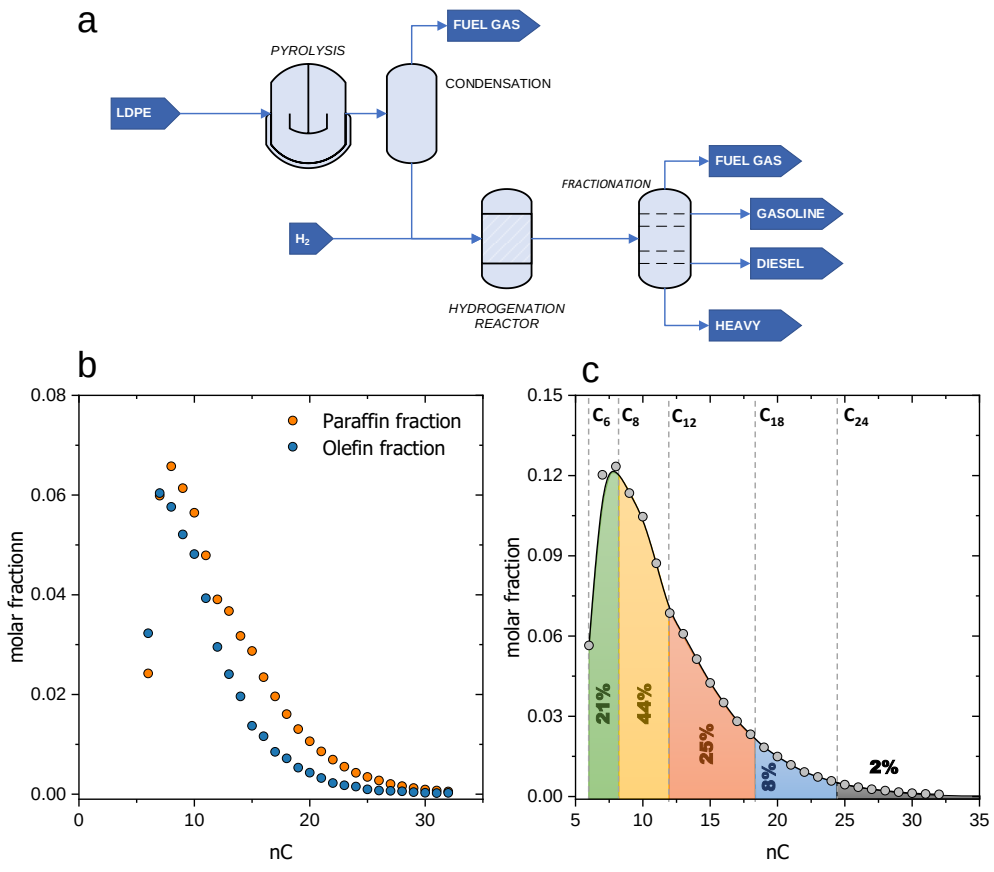

130

131 **Figure 1.** Composition of the liquids of pyrolysis of LDPE [21]. (a) Diagram of the process; (b) Molar
132 fraction as a function of the carbon number of the olefin and paraffin fractions; (c) Total molar fraction as
133 a function of the carbon number.

134 **Table 1.** Properties analyzed for the pyrolysis liquids (PL) from different pyrolysis batches and some
135 requirements for automotive diesel (class A) according to European legislation [42].

		Regulatory Limits						
Property	**Test method**	**min.**	**max.**	**PL1**	**PL2**	**PL3**	**PL4**	**PL5**
Density at 15 ºC (kg/m^3)	ASTM D 4052-18a [43]	820	845	783	793	799	805	791
Flash point (ºC)	ASTM D 93-18 [44]	55	-	< 25	< 25	< 25	< 25	< 25
Oxidative stability (h)	EN 15751:2014 [45]	20	-	18.1	20.1	*	*	*
Sulphur content (mg/kg)	EN 20846:2011 [46]	-	10	12.4	12.9	19.0	16.8	4.4
Bromine number (g Br_2/100 g sample)	ASTM D1159-07(2017) [47]	-	-	32.0	39.6	40.0	37.0	31.0

* It was not possible to complete the test due to gum formation so the samples do not meet with this parameter

Table 1 summarizes the most important fuel properties required by international regulations together with the bromine number, which is a representative measurement of the content in olefinic double bonds present in a sample [48]. Considering the results in Table 1, it can be concluded that a traditional distillation step is necessary to obtain a hydrocarbon fraction in the diesel range that meets some parameters required by standards (i.e. density and flash point). However, the distillation step is not enough to improve other properties such as sulphur content, oxidative stability, and the bromine number. The last two parameters are related to the tendency of the olefins to form gums in the engine. All these properties could be improved using an upgrading treatment of the pyrolysis liquids, and then the distillation stage.

2.2. CFD model description

The CFD model was built in Comsol Multiphysics v4.4. The olefin hydrogenation process is proposed to be carried out in a multi-tubular fixed-bed reactor (Figure 2) equipped with 37 catalyst-filled tubes within a shell, in which a heat transfer fluid circulates. Considering that the hydrogenation reactions in the tube catalyst beds are exothermic, thermal oil is used as a cooling fluid to provide optimal heat control and isothermal conditions, avoiding the occurrence of hotspots. The synthetic heat transfer fluid (DIPHYL ®) is a eutectic mixture of 73.5 % diphenyl oxide (DPO) and 26.5 % diphenyl. The temperature range for its use in liquid phase is 12 to 400 ºC. As can be seen in Figure 2, the internal diameter of the reactor shell is 344 mm and each reactor tube is 38 mm in internal diameter and 2000 mm in length.

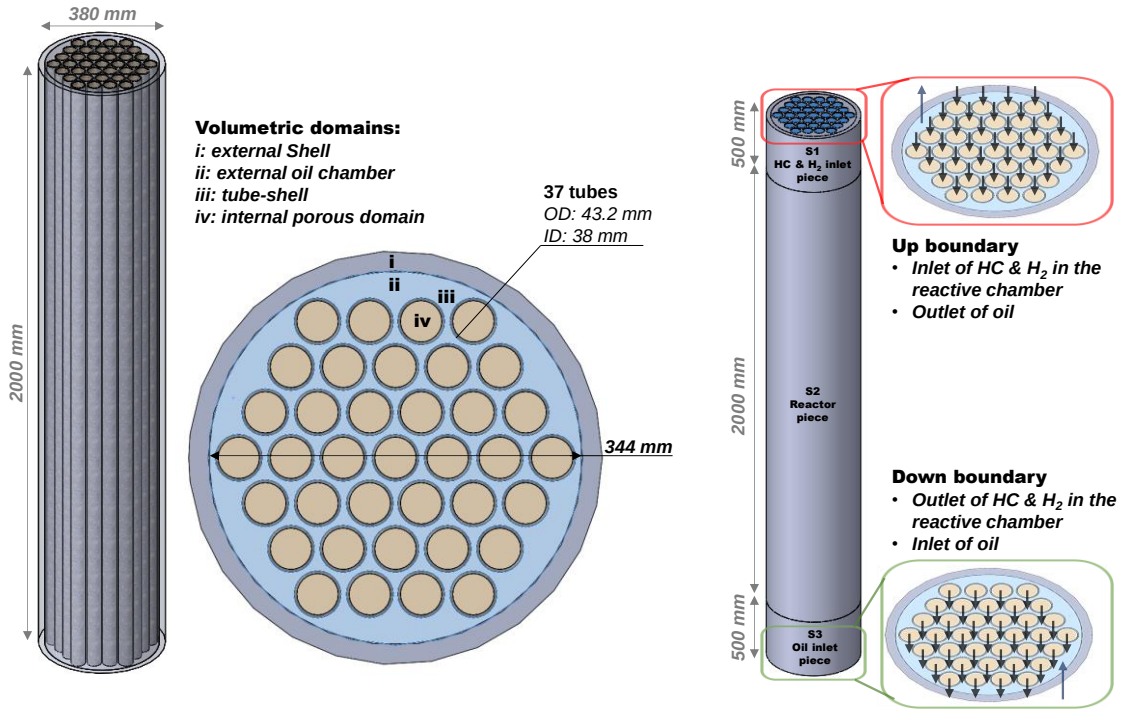

159

160 **Figure 2.** Setup used for the hydrogenation of olefins - Dimensions.

161

162 The fluid flow was modelled by means of Navier-Stokes equations with the Brickman
163 correction for the catalytic porous medium of the internal tube domains (Table 2; eqs. 1-
164 4 and 12-15). Regarding gas diffusion, the species transport phenomena were calculated
165 with the average mixture method based on Maxwell-Stefan equations (Table 2; eqs. 5-7
166 and 16-18), and considering hydrogen and all the olefin and paraffin species (Figure 1).
167 The diffusion coefficient was corrected by the ratio between the porosity and the porous
168 bed tortuosity. The porosity and permeability are two key factors that govern the fluid
169 flow in the porous region and the permeability for a packed bed with randomly distributed
170 spherical particles. Both parameters were calculated using the Carman-Kozeny model and
171 the stated particle size and porosity model [49]. Additionally, the tortuosity of the system
172 was evaluated considering the inverse of the square root of the porosity of the domain,
173 and considering the catalyst as a packed bed with randomly distributed spherical particles

174 [50,51]. The porous bed was modelled considering spherical particles of 1 mm and 40 %

175 of porosity. Pure gas properties were obtained from the literature [52].

176

177 **Table 2.** Ruling equations of the different phenomena taking place in the olefin hydrogenation process.

Ruling equations	Eq.	Properties	Eq.
Fluid transport			
$\rho(u\cdot\nabla)u=\nabla\cdot\left[-pI+\mu(\nabla u+(\nabla u)^r-\frac{2}{3}\mu(\nabla\cdot u)I\right]$	(1)	$\rho=\frac{p}{R\cdot T}\cdot M_n$	(12)
$\nabla\cdot(\rho u)=0$	(2)	$\mu=\sum_i\frac{\mu_{g,i}}{1+\frac{1}{x_i}\cdot\sum_{j,j\neq i}x_j\cdot\phi_{i,j}}$	(13)
$\frac{\rho}{\epsilon_p}\left((u\cdot\nabla)\frac{u}{\epsilon_p}\right)=\nabla\cdot\left[-pI+\frac{\mu}{\epsilon_p}(\nabla u+(\nabla u)^r)-\frac{2\mu}{3\epsilon_p}(\nabla\cdot u)I\right]-\left(\mu\kappa^{-1}+\beta_F\lvert u\rvert+\frac{Q_{br}}{\epsilon_p^2}\right)u$	(3)	$\phi_{i,j}=\frac{\left(1+\left(\frac{\mu_{g,i}}{\mu_{g,i}}\right)^{\frac{1}{2}}\cdot\left(\frac{M_j}{M_i}\right)^{\frac{1}{4}}\right)^2}{\frac{4}{\sqrt{2}}\cdot\left(\frac{M_j}{M_i}\right)^{\frac{1}{2}}}$	(14)
$\nabla\cdot(\rho u)=Q_{br}$	(4)	$\kappa=\frac{d_p^2\cdot\epsilon_p^3}{180\cdot(1-\epsilon_p)^2}$	(15)
Diffusive transport			
$\nabla\cdot j_i+\rho(u\cdot\nabla)w_i=r_i\cdot M_i$	(5)	$D_i^m=\frac{1-w_i}{\sum_{\kappa\neq i}\frac{x_k}{D_{i,\kappa}}}$	(16)
$N_i=j_i+\rho u w_i$	(6)	$M_n=\left(\sum_i\frac{w_i}{M_i}\right)^{-1}$	(17)
$j_i=-\left(\rho D_i^m\nabla w_i+\rho w_i D_i^m\frac{\nabla M_n}{M_n}\right)$	(7)	$D_{i,j}=k_{dif\,f}\cdot\frac{T^{1,75}\cdot\left(\frac{1}{M_i}+\frac{1}{M_j}\right)^{1/2}}{p\cdot\left(v_i^{1/3}+v_j^{1/3}\right)^2}$	(18)
Heat transport			
$\rho Cpu\cdot\nabla T=\nabla(k\cdot\nabla T)+Q_{term}$	(8)	$k=\sum_i\frac{k_{g,i}}{1+\frac{1}{x_i}\cdot\sum_{j,j\neq i}x_j\cdot\phi_{i,j}}$	(19)
$\rho Cpu\cdot\nabla T=\nabla(keq\cdot\nabla T)+Q_{term}$	(9)	$keq=\theta_p\cdot k_p+\left(1-\theta_p\right)\cdot k$	(20)
$Heat_{ri}=-r_i\cdot\Delta H_{ri}$	(10)	$Cp=\sum_i x_i\cdot Cp_{g,i}$	(21)
		$\gamma=\sum_i x_i\cdot\gamma_{g,i}$	(22)
Kinetic model			
$r_{OLE,i}=k\cdot C_{OLE,i}$	(11)	$k=k_0\cdot exp\left(-\frac{Ea}{R\cdot T}\right)$	(23)

178

Table 3. Phenomena considered in each volume domain.

		Fluid flow		Gas diffusion		Chemical reactions	Heat transport	
Piece	**Domain**	**Navier-Stokes**	**Brickman**	**Free**	**Porous**		**Free**	**Porous correction**
S1	**i**	×	×	×	×	×	✓	×
	ii	✓	×	✓	×	×	✓	×
	iii	×	×	×	×	×	✓	×
	iv	✓	×	✓	×	×	✓	×
S2	**i**	×	×	×	×	×	✓	×
	ii	✓	×	✓	×	×	✓	×
	iii	×	×	×	×	×	✓	×
	iv	×	✓	×	✓	✓	×	✓
S3	**i**	×	×	×	×	×	✓	×
	ii	✓	×	✓	×	×	✓	×
	iii	×	×	×	×	×	✓	×
	iv	✓	×	✓	×	×	✓	×

Gas density was calculated considering ideal gas mixtures (Table 2; eq. 12). The viscosity and the thermal conductivity for the gas mixtures (both internal and external gas mixtures) were calculated using the Wilke model (Table 2; eqs. 13, 14 and 19). The heat capacity and the heat capacity ratio for gas mixtures were estimated considering the molar average (Table 2; eqs. 21 and 22). Both governing equations and properties have been summarized in Table 2. Table 3 shows the type of phenomena considered in the different domains of each piece, as defined in Figure 2.

Kinetic data for the olefin hydrogenation reaction used in the model were adapted from the kinetic model obtained by Fan et al. [53]. These authors used a bifunctional catalyst based on Ni-Mo typical of hydrogenation processes [48,54]. Taken into account that the olefin hydrogenation process is exothermic, one of the most important factors for the reactor design is the management of the heat released [55]. To that end, cooled multi-tubular reactor has been selected in this study because it is well-established and widely used in chemical industry for this purpose [56]. The modelled reactor is cooled by a counter-current stream of thermal oil on the shell side and the catalyst is put inside the tubes in a packed-bed. As a starting point and according to the processing capacity of the

198 Urbaser pilot plant (PtO technology), the length and internal diameter established for the
199 tubes of the new hydrotreatment unit are 2000 mm and 38 mm, respectively.
200
201 To simulate the composition of the LDPE pyrolysis liquids, five olefin/paraffin
202 compounds were chosen based as depicted in Figure 1c. The olefin components comprise:
203 1-hexene (C_6H_{12}), 1-octene (C_8H_{16}), 1-dodecene ($C_{12}H_{24}$), 1-octadecene ($C_{18}H_{36}$), and 1-
204 tetracosene ($C_{24}H_{48}$). Paraffin compounds include: hexane (C_6H_{14}), octane (C_8H_{18}),
205 dodecane ($C_{12}H_{26}$), octadecane ($C_{18}H_{38}$), and tetracosane ($C_{24}H_{50}$). From the paraffins,
206 olefins, naphthenes, and aromatics (PONA) analysis, the olefin/paraffin ratio (in mass) in
207 the pyrolysis liquids was obtained (0.40). The couple of olefin/paraffin was simulated
208 using this value. The composition of the different hydrocarbons follows the distribution
209 showed in Figure 1b.
210
211 Typical hydrotreatment process conditions [53,57] were fixed initially to obtain overall
212 results of the reactor performance, and to establish a basis for the sensitivity analysis. The
213 conditions of the baseline scenario are summarized in Table 4. The range of the different
214 variables studied in the sensitivity analysis is indicated in section 2.3. Note that the value
215 of the rest of parameters is the same as shown in Table 4.
216

Table 2. Initial conditions fixed in the baseline scenario.

System parameter	Unit	Initial value
Pyrolysis liquid flow (F)	kg/h	0.83 each tube
Initial olefin mass fraction (χ_{OLE})	-	0.40
Thermal oil flow	L/h	20
Catalyst mass (W)	kg	0.2
Spatial time (W/F)	h	0.24
H_2/pyrolysis liquid ratio (H_2/HC)	NL/L	400
Reactor inlet temperature	º C	375
Hydrogen pressure	barg	40
Thermal oil heat transfer coefficient (h)	W/m^2K	51
Thermal oil inlet temperature	º C	375

2.3. Sensitivity analysis

2.3.1. Effect of the spatial time

The effect of the spatial time (W/F) was evaluated in the range of 0.1-0.6 h (where W is the amount of catalyst in unit of kg, and F is the mass flow rate of pyrolysis liquids in unit of kg/h). The catalyst load (W) was varied in order to keep the H_2/pyrolysis liquid ratio in 400 NL/L. The results are compared to data obtained from experimental tests.

2.3.2. Effect of heat transfer fluid flow

Thermal oil was tested in the range from 0.1 to 10 m^3/h. The solution was compared with a 0D heat balance. This 0D approach solves the temperature (T) comparing the reaction heat with the heating energy of the inlet stream (eq. 24).

$$\sum_i\left(-\Delta H_{r_i}\cdot r_i\right)=\sum_i m_i\cdot\int_{T_{inlet}}^{T} cp_i(T)dT \quad (24)$$

2.3.3. Effect of H_2/pyrolysis liquid ratio

The influence of the hydrogen to pyrolysis liquid ratio was studied in the range of 100-500 NL/L (keeping the pyrolysis liquid flow in 30.71 kg/h). This study allowed the evaluation of the hydrogen demand of the hydrotreatment process.

2.4. Meshing and solver

The mesh performed for each domain was based on triangular elements (Figure 3). The element size was calibrated for fluid dynamics. The average mesh quality used was 0.55. Near the tubes boundary, the mesh was refined to have a finer mesh. The overall mesh contains 2519539 tetrahedra elements (31.5 % in the oil domain, 35.3 % in the shell and the tubes, and the 33.2 % in the internal reactive domain).

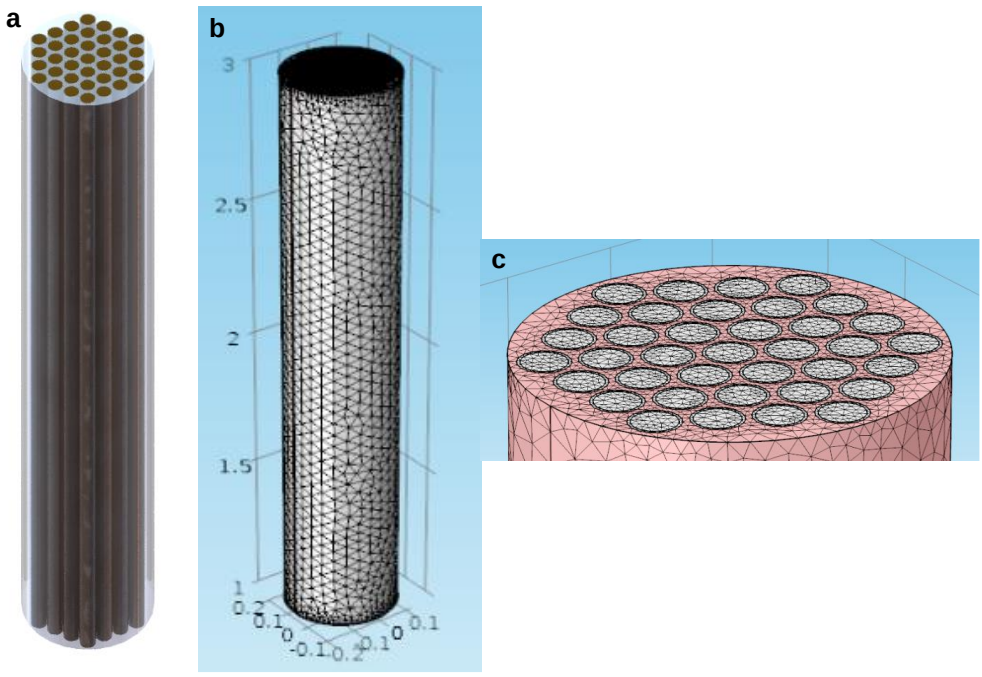

Figure 3. 3D model with 37 tubes and exterior shell. a) Complete view of the reactor; b) Complete view of the mesh; c) Detailed view of the mesh.

Calculations were carried out using the Parallel Direct Solver (PARDISO) in steady state mode with parameter continuation to facilitate convergence. The relative tolerance of the method was 0.001. Consistent stabilization criterion was chosen for all phenomena using streamline diffusion and crosswind diffusion.

2.5. Thermodynamic methods

In addition to the CFD study, the thermodynamic evaluation of gas condensability was analyzed. In this sense, a biphasic system (gas – liquid) in an isothermal process was considered. Different thermodynamic systems were employed by means of a commercial software ASPEN PLUS V 10.0 [58]. Recommended advanced models for refinery applications with high hydrogen content were used. These models include: Peng-Robinson, Soave-Redlich-Kwong equation of state with temperature dependency (SRK), Redlich-Kwong-Soave (RK-SOAVE), and Redlich-Kwong-Soave with Boston-Mathias alpha function (RKS-BM) [59]. As described in Figure 1c, the compounds used for this study include hydrogen, and n-paraffins and olefins ranging from 6 (C6) to 24 (C24) carbon atoms, as a representative composition of the LDPE pyrolysis liquids. The distribution of the hydrocarbon mixture is shown in Figure 1b. It is important to note that the condensation of the mixture of H_2 and pyrolysis liquids can occur more easily when the full olefin conversion is achieved. Considering this, the condensation effect has been evaluated using a mixture of hydrogen and n-paraffins ranging from 6 (C6) to 32 (C32) carbon atoms (considering the specific composition of the liquid viewed in the Figure 1). To that end, a flash separation unit was used at 375°C and the specified pressure. The effect of the total pressure was studied in the range of 40-100 bar at a given hydrogen to pyrolysis liquid ratio of 400 NL/L. The influence of the hydrocarbon dilution was evaluated at 40 bar, varying the hydrogen to pyrolysis liquid ratio from 50 to 550 NL/L.

3. Results and discussion

The described model was evaluated to orientate the design of the catalytic reactor to be integrated in the Urbaser pilot plant, and the optimal operating conditions of the olefin hydrogenation process. For this purpose, first a comparison of the model with experimental data was made in isothermal conditions. Then, the model was used to evaluate the adiabatic process. Finally, as the condensation of hydrocarbons (especially, the heavier compounds) was not evaluated in the CFD model, a thermodynamic evaluation was performed to select between the optimal conditions coming from the CFD model and the most suitable conditions that allows to avoid undesired condensation inside the hydrogenation reactor. The optimal conditions of the process were also established based on the specifications of the materials for the reactor.

3.1. CFD results

The CFD model requires an initial step to validate the results provided by the tool. In this case, the evaluation was made by comparing the experimental data in isothermal conditions and the results obtained from the CFD model. Figure 4 shows the comparative results of the olefin conversion (Figure 4a) and the profile of the olefin weigh fraction (Figure 4b) for the different spatial times analyzed. As expected, an increase in the spatial time values results in an increase in the olefin conversion. Note that the experimental data fitted CFD model properly (Figure 4a). As can be observed, the full olefin conversion is reached when the spatial time is higher than 0.3 h. According to the profile (Figure 4b), olefins are being hydrogenated in the first zones of the reactor. The reaction is gradually deactivated (especially for the lowest spatial times) due to the decrease of the activity of the olefins as they are consumed. Specifically, the evolution of olefin mass fraction along

the tube indicates that complete olefin conversion to paraffinic species is achieved before reaching the middle of the tube (1000 mm from the inlet). Considering this result, a 1000 mm length reactor would be enough to carry out the hydrogenation process since no more conversion will be achieved with additional length.

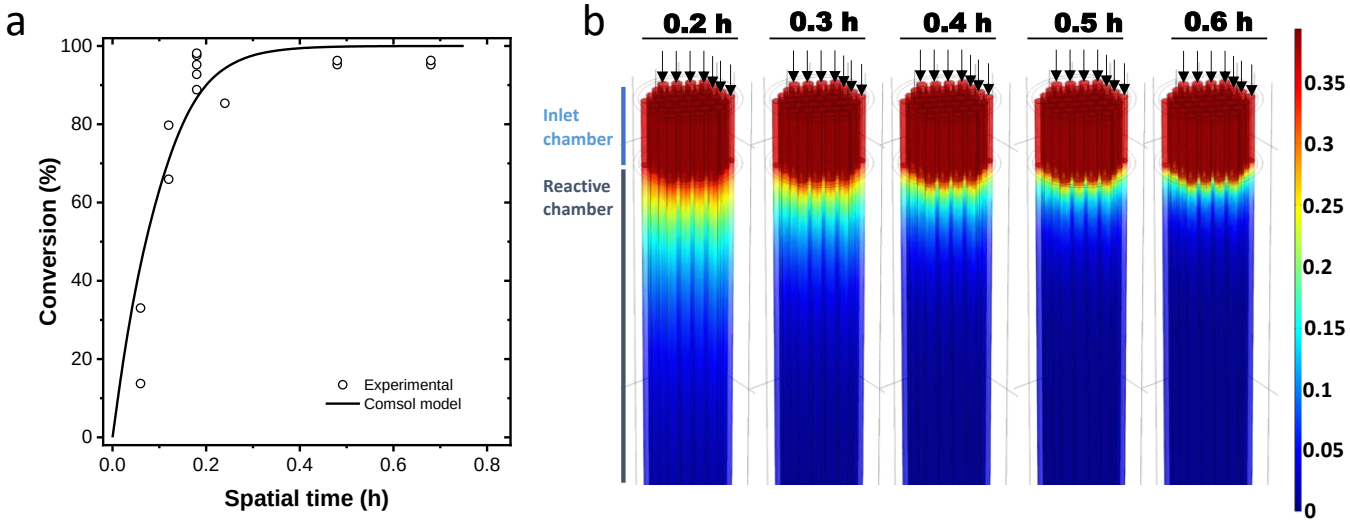

Figure 4. Validation of the CFD model. (a) Comparison of the olefin conversion as a function of the spatial time between the experimental data and CFD model; (b) Olefin weight fraction profiles for different spatial times. 375 °C, 20 L/h of oil, H_2/HC: 400 NL/L.

The same analysis was made in adiabatic conditions. The temperature profiles (Figure 5) for the different spatial times analyzed reveal that the heat is gathered in the first zone of the reactor (where the main fraction of olefins is reacting) and in the center. In all cases, the temperature increase is lower than 40 °C. Therefore, it can be corroborated that the oil used as a heat transfer fluid allows to keep the temperature under control, minimizing temperature gradients within the reactor volume.

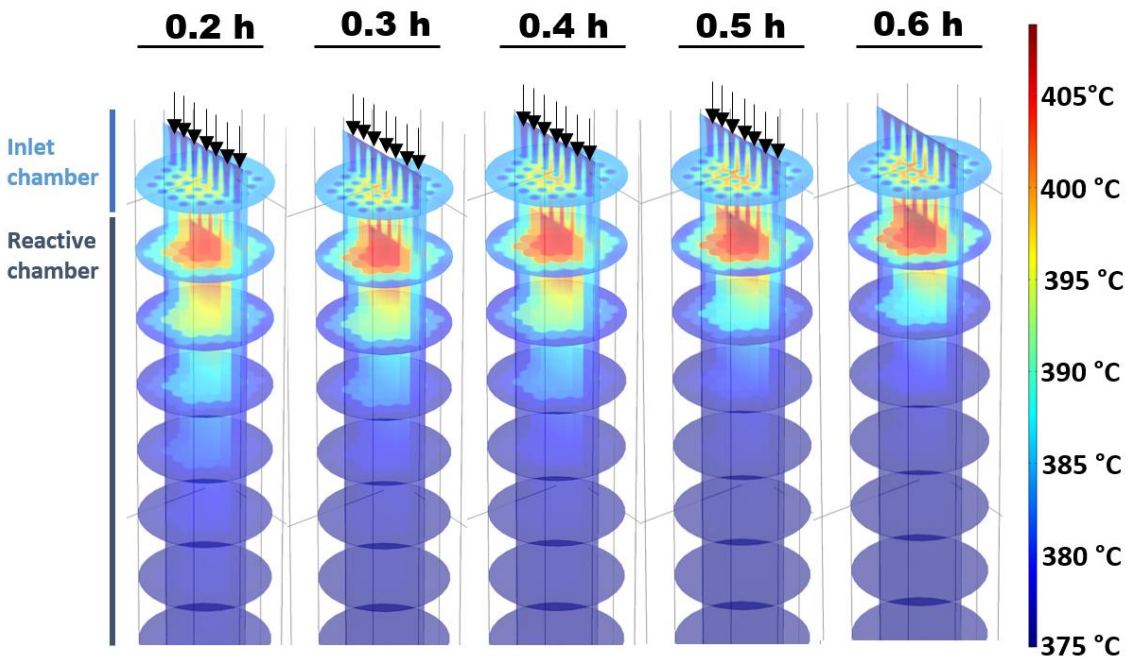

Figure 5. Temperature profiles for different spatial times. Inlets at 375 °C, 20 L/h oil, H_2/HC: 400 NL/L.

In addition, a comparison with a 0D heat balance was made in order to assess the validity of the adiabatic studies performed. It is important to note that the counter-flow configuration of the reactor is not considered by the 0D model. The results in Figure 6 show that the maximum temperatures reached in the 3D Comsol model (counter-flow distribution) are similar to the 0D heat balance (overall balance). Considering the results of the temperature distribution (Figure 6b), it can be concluded that the temperature gradients are completely mitigated when the flow of refrigerant oil reaches values of about 0.5 m^3/h. The increase in the oil flow leads to a decrease in temperature in the first zone of the reactor, and thus kinetic activity decreases. This is why more reactor length is needed to achieve full olefin conversion as the oil flow is increased. However, for all cases this increase in the reaction length is low because complete olefin conversion is achieved before the mid-length of the reactor. Additionally, the increase in the flow of refrigerant oil results in a better distribution of the reaction heat because the oil has a larger area to absorb the released energy.

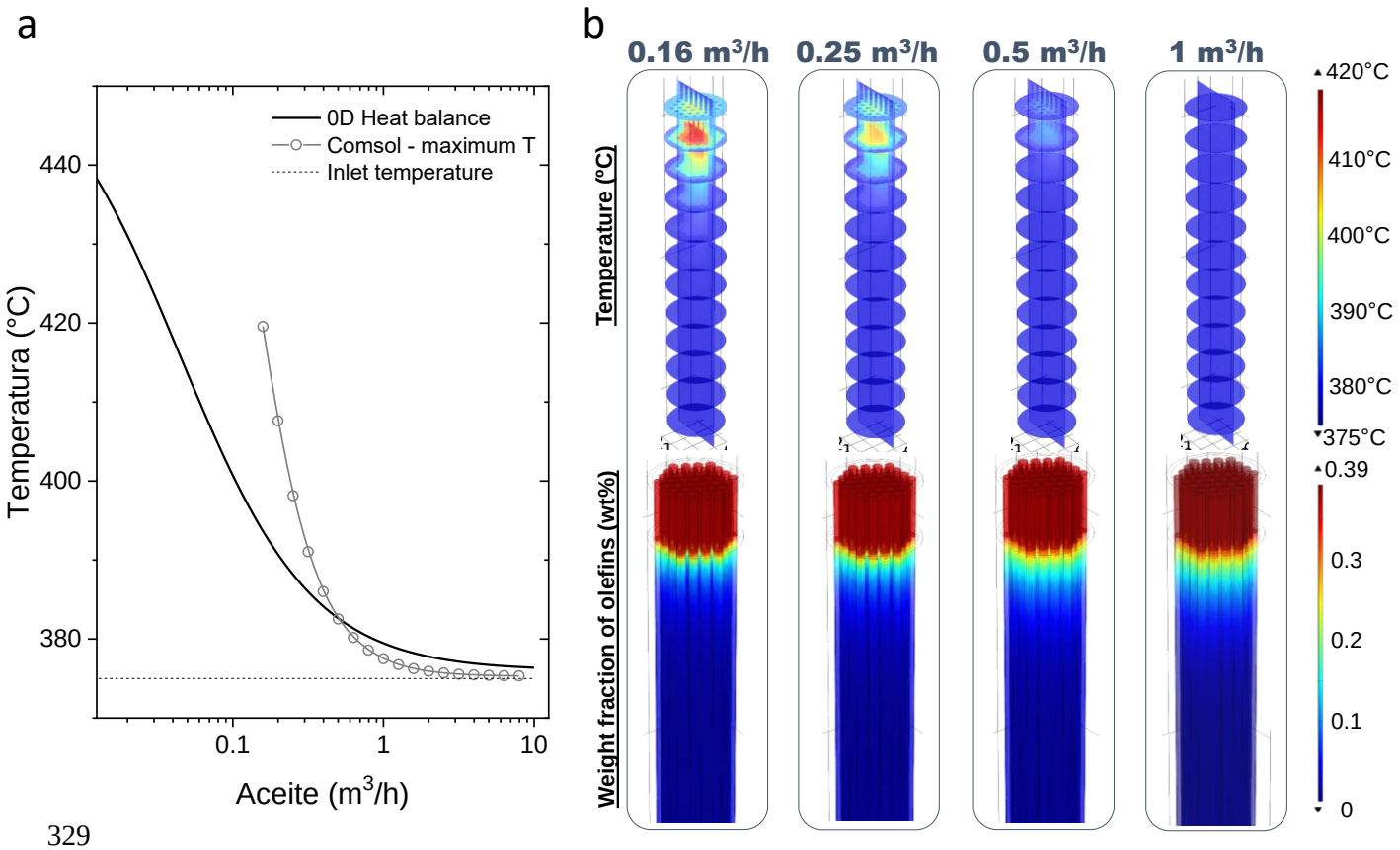

Figure 6. Effects of the oil flow. (a) Comparison between the 0D heat balance and the Comsol model results. (b) Temperature profiles for different oil flows; (c) Weight fraction of the olefin for different oil flow. Inlets at 375 °C, spatial time 0.48 h, H_2/HC: 400 NL/L.

The increase in the hydrogen/pyrolysis liquid ratio could cause a mitigation of temperature gradients since there is a higher amount of matter to be heated and there is a decrease in the olefin concentration by a diluting effect, and thus a decrease in the kinetic activity. Figure 7 shows the results of the variation of the H_2 feeding in adiabatic conditions. The study considers the adiabatic model varying the H_2/HC ratio between 100 and 400 NL/L. In absolute terms, both trends are confirmed: (1) decrease in the temperature, and (2) decrease in the kinetic activity. However, the differences are less important than the effect of the spatial time or the refrigerant oil flow.

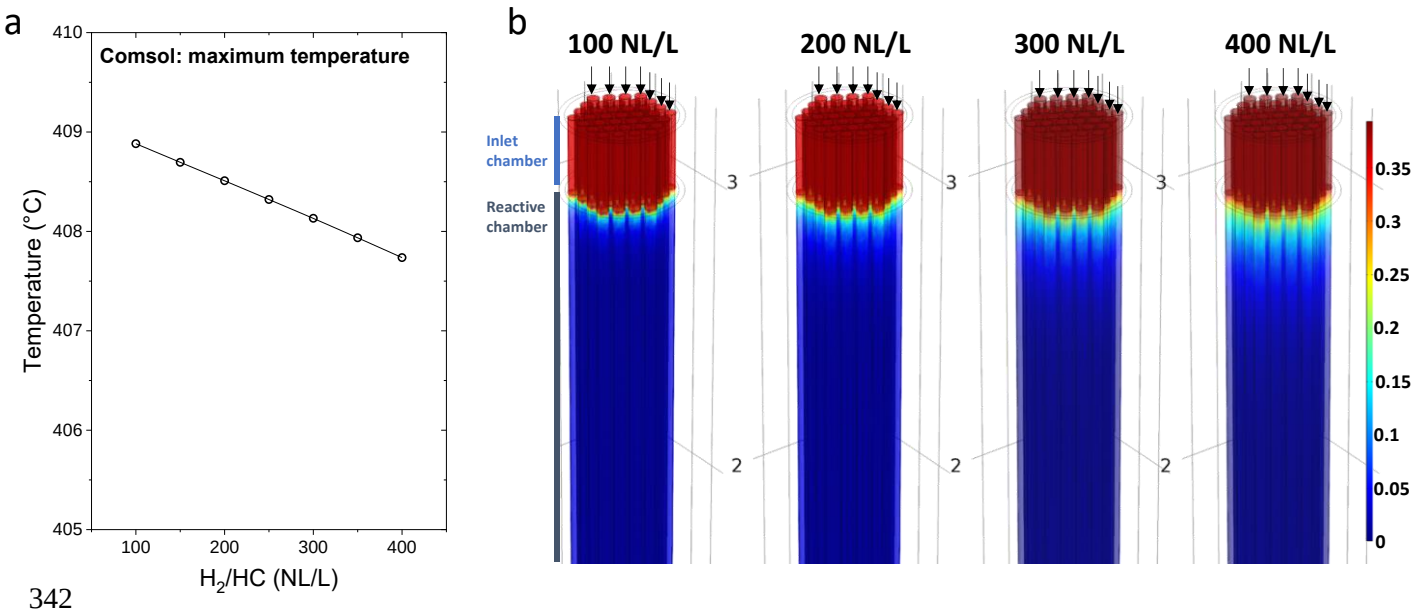

342

343 **Figure 7.** Results of the effect of the H_2/HC ratio in the inlet stream. (a) Maximum temperature reached on
344 the reactor as a function of the H_2/HC ratio in the feed stream. (b) Temperature profiles for different H_2/HC
345 ratios in the feed stream. Inlets at 375 °C, spatial time 0.48 h, oil flow 20 L/h.

346

347 *3.2. Thermodynamic evaluation of the condensation*

348 Condensability of the stream components has been evaluated considering different
349 thermodynamic systems for the liquid-gas equilibrium. Taking into account the reactive
350 stream, the heavier fractions present its maximum activity in the outlet stream (as
351 paraffins). Therefore, the evaluation was made considering that hydrocarbons in this
352 stream are in the form of paraffins. Figure 8 shows the results of this analysis. As can be
353 observed (Figure 8a), the condensations can be avoided if the total pressure of the reactive
354 chamber is below 45 bar. Additionally, an increase in the H_2/HC ratio leads to the dilution
355 of the hydrocarbon fractions, and thus their activity decreases. Therefore, the presence of
356 liquid inside the reactor can be avoided using values of the H_2/HC ratio above 350 NL/L
357 (Figure 8b).

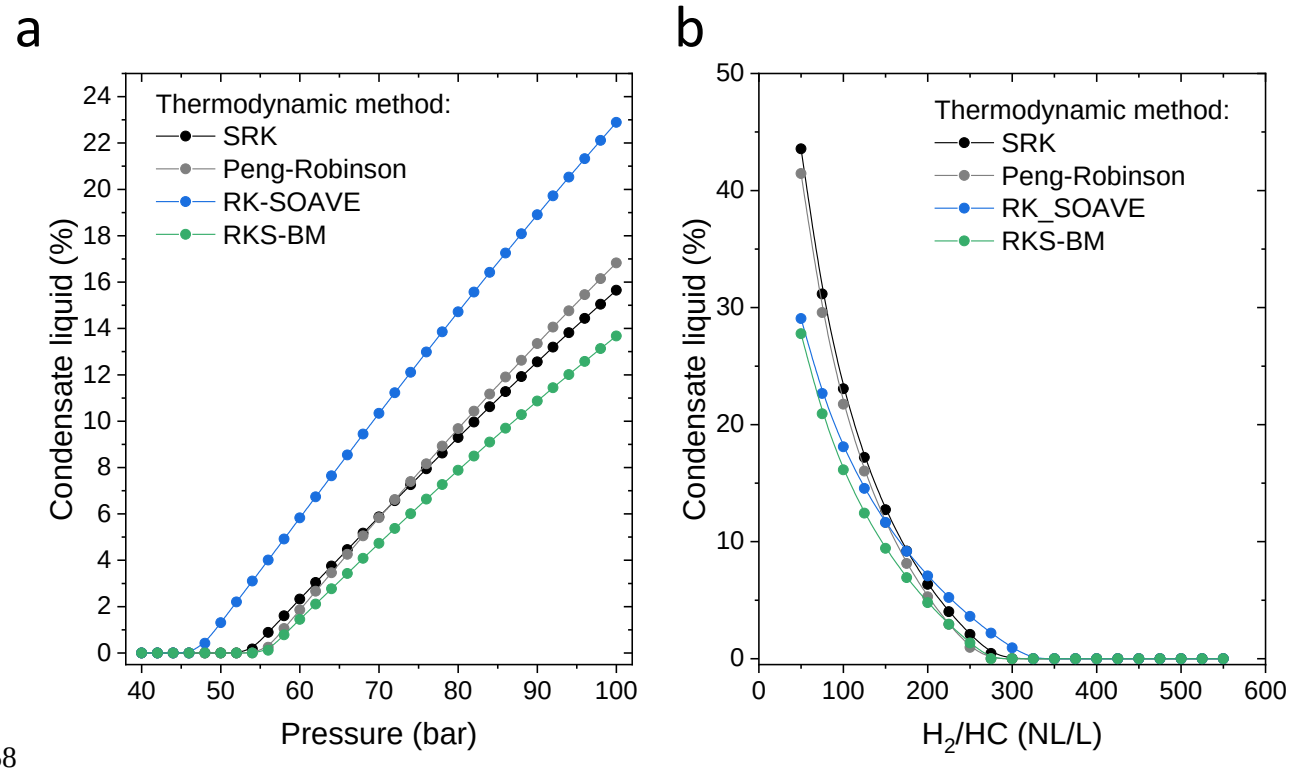

358

359 **Figure 8.** (a) Condensed liquid as a function of total pressure (H_2/feedstock ratio: 400 NL/L); (b)
360 Condensed liquid as a function of the H_2/HC ratio (pressure: 40 bar). SRK: Soave-Redlick-Kwong; RK-
361 SOAVE: Redlich-Kwong-Soave; RKS-BM: Redlich-Kwong-Soave with Boston-Mathias alpha function.

362

363 This conclusion about the pressure and the confirmation that heat transfer fluid allows to
364 keep the temperature under 375 ºC have been used to establish the catalytic reactor
365 material. Based on the results obtained in this study, A-316L austenitic stainless steel has
366 been selected as building material for the reactor. This material is widely used in pressure
367 vessels for its excellent mechanical properties [60]. Considering this material and the
368 proposed design for the reactor, the maximum allowable pressure is 50 bar in the tubes
369 and 16 bar in the shell-side, and the maximum allowable temperature is 400 °C. Note that
370 these limits are above the process conditions with an acceptable security margin to carry
371 out the hydrogenation reactions.

372

4. Conclusions

CFD analysis has been used to establish the design of a new catalytic hydrotreatment reactor as a preliminary step to its construction and integration into an existing pilot plant of plastic waste valorization. The catalytic reactor has been designed as a multi-tubular fixed-bed reactor equipped with 37 catalyst-filled tubes within a shell, in which a heat transfer fluid circulates. As a general conclusion, the results of the proposed 3D model confirm that the pilot reactor design will allow to carry out the exothermic hydrogenation reaction of LDPE pyrolysis liquids (>30 kg/h) properly, without building large temperature gradients within the reactor volume. The use of heat transfer oil (DIPHYL®) in the pilot plant enabled good temperature control in the reactor, leading to nearly-isothermal conditions. In addition, Comsol model provides some basic guidelines in order to decide the final dimensions of the reactor and the operating conditions:

- A 1000 mm length reactor would be enough to carry out the hydrogenation process with an excellent control over the outlet temperature.
- If total conversion is desired, it is highly recommendable to work at spatial times higher than 0.3 h.
- In all the conditions studied, the increase in temperature is lower than 40 °C, confirming that the refrigerant oil used allows to keep the temperature under control. Thermal oil flow has been checked by comparing with the 0D heat balance.
- The H_2/pyrolysis liquid ratio influences the conversion of olefins, but to a lesser extent than refrigerant oil flow or spatial time.
- The increases in total pressure and H_2/pyrolysis liquid ratio lead to a higher probability of liquid condensation. However, condensation problems can be

avoided by keeping the total pressure of the reactive chamber below 45 bar and using H_2/pyrolysis liquid ratios above 350 NL/L.

Moreover, CFD analysis has provided enough information about the critical variables of the process (temperature and pressure) to select the reactor material. A combination of up to 50 bar and 400 ºC could be achieved using A-316L steel for the construction of the reactor. Taking into account these limits, the CFD model results (predicting an outlet temperature under 375 ºC) and the thermodynamic evaluation of the condensation (recommending pressures under 45 bar), the viability of the hydrogen process scaling up has been shown.

Acknowledgements

The authors acknowledge the financial support of the Centre for the Development of Industrial Technology [grant number IDI – 20150730] and the Ministerio de Ciencia, Innovación y Universidades (Spain) [grant number DI – 16 – 08700]

References

[1] Europe P. Plastics - the Facts 2019. An analysis of European plastics production, demand and waste data. 2019.

[2] Rochman CM, Browne MA, Halpern BS, Hentschel BT, Hoh E, Karapanagioti HK, et al. Policy: Classify plastic waste as hazardous. Nature 2013;494:169–70. https://doi.org/10.1038/494169a.

[3] Brems A, Baeyens J, Dewil R. Recycling and recovery of post-cet alonsumer plastic solid waste in a European context. Therm Sci 2012;16:669–85.

https://doi.org/10.2298/TSCI120111121B.

[4] Heydariaraghi M, Ghorbanian S, Hallajisani A, Salehpour A. Fuel properties of the oils produced from the pyrolysis of commonly-used polymers: Effect of fractionating column. J Anal Appl Pyrolysis 2016;121:307–17. https://doi.org/10.1016/j.jaap.2016.08.010.

[5] Lazarevic D, Aoustin E, Buclet N, Brandt N. Plastic waste management in the context of a European recycling society: Comparing results and uncertainties in a life cycle perspective. Resour Conserv Recycl 2010;55:246–59. https://doi.org/10.1016/j.resconrec.2010.09.014.

[6] Comission E. EU Circular Economy Action Plan. A new Circular Economy Action Plan for a Cleaner and More Competitive Europe 2020.

[7] Panda AK, Singh RK, Mishra DK. Thermolysis of waste plastics to liquid fuel. A suitable method for plastic waste management and manufacture of value added products-A world prospective. Renew Sustain Energy Rev 2010;14:233–48. https://doi.org/10.1016/j.rser.2009.07.005.

[8] Singh RK, Ruj B, Sadhukhan AK, Gupta P, Tigga VP. Waste plastic to pyrolytic oil and its utilization in CI engine: Performance analysis and combustion characteristics. Fuel 2020;262:116539. https://doi.org/https://doi.org/10.1016/j.fuel.2019.116539.

[9] Anuar Sharuddin SD, Abnisa F, Wan Daud WMA, Aroua MK. A review on pyrolysis of plastic wastes. Energy Convers Manag 2016;115:308–26. https://doi.org/https://doi.org/10.1016/j.enconman.2016.02.037.

[10] Lopez G, Artetxe M, Amutio M, Bilbao J, Olazar M. Thermochemical routes for the valorization of waste polyolefinic plastics to produce fuels and chemicals. A

review. Renew Sustain Energy Rev 2017;73:346–68. https://doi.org/https://doi.org/10.1016/j.rser.2017.01.142.

[11] Kalargaris I, Tian G, Gu S. The utilisation of oils produced from plastic waste at different pyrolysis temperatures in a DI diesel engine. Energy 2017;131:179–85. https://doi.org/10.1016/j.energy.2017.05.024.

[12] Bagri R, Williams PT. Catalytic pyrolysis of polyethylene. J Anal Appl Pyrolysis 2002;63:29–41. https://doi.org/https://doi.org/10.1016/S0165-2370(01)00139-5.

[13] Marcilla A, Beltrán MI, Navarro R. Thermal and catalytic pyrolysis of polyethylene over HZSM5 and HUSY zeolites in a batch reactor under dynamic conditions. Appl Catal B Environ 2009;86:78–86. https://doi.org/https://doi.org/10.1016/j.apcatb.2008.07.026.

[14] Uddin MA, Koizumi K, Murata K, Sakata Y. Thermal and catalytic degradation of structurally different types of polyethylene into fuel oil. Polym Degrad Stab 1997;56:37–44. https://doi.org/10.1016/S0141-3910(96)00191-7.

[15] Onwudili JA, Insura N, Williams PT. Composition of products from the pyrolysis of polyethylene and polystyrene in a closed batch reactor: Effects of temperature and residence time. J Anal Appl Pyrolysis 2009;86:293–303. https://doi.org/https://doi.org/10.1016/j.jaap.2009.07.008.

[16] Sakata Y, Uddin MA, Muto A. Degradation of polyethylene and polypropylene into fuel oil by using solid acid and non-acid catalysts. J Anal Appl Pyrolysis 1999;51:135–55. https://doi.org/https://doi.org/10.1016/S0165-2370(99)00013-3.

[17] Su J, Fang C, Yang M, You C, Lin Q, Zhou X, et al. Catalytic pyrolysis of waste packaging polyethylene using AlCl3-NaCl eutectic salt as catalyst. J Anal Appl Pyrolysis 2019;139:274–81. https://doi.org/10.1016/j.jaap.2019.02.015.

[18] Williams EA, Williams PT. The pyrolysis of individual plastics and a plastic mixture in a fixed bed reactor. J Chem Technol Biotechnol 1997;70:9–20. https://doi.org/10.1002/(SICI)1097-4660(199709)70:1<9::AID-JCTB700>3.0.CO;2-E.

[19] Yan G, Jing X, Wen H, Xiang S. Thermal cracking of virgin and waste plastics of PP and LDPE in a semibatch reactor under atmospheric pressure. Energy and Fuels 2015;29:2289–98. https://doi.org/10.1021/ef502919f.

[20] Zhou Q, Zheng L, Wang YZ, Zhao GM, Wang B. Catalytic degradation of low-density polyethylene and polypropylene using modified ZSM-5 zeolites. Polym Degrad Stab 2004;84:493–7. https://doi.org/10.1016/j.polymdegradstab.2004.01.007.

[21] Gala A, Guerrero M, Guirao B, Domine ME, Serra JM. Characterization and Distillation of Pyrolysis Liquids Coming from Polyolefins Segregated of MSW for Their Use as Automotive Diesel Fuel. Energy & Fuels 2020. https://doi.org/10.1021/acs.energyfuels.0c00403.

[22] Serrano DP, Escola JM, Briones L, Arroyo M. Hydroprocessing of the LDPE thermal cracking oil into transportation fuels over Pd supported on hierarchical ZSM-5 catalyst. Fuel 2017;206:190–8. https://doi.org/https://doi.org/10.1016/j.fuel.2017.06.003.

[23] Joo HS, Guin JA. Continuous upgrading of a plastics pyrolysis liquid to an environmentally favorable gasoline range product. Fuel Process Technol 1998;57:25–40. https://doi.org/10.1016/S0378-3820(98)00067-8.

[24] (CEN) EC for S. Automotive Fuels – Diesel - Requirements and Test Methods 2017;00019524.

[25] Priharto N, Ronsse F, Prins W, Hita I, Deuss PJ, Heeres HJ. Hydrotreatment of pyrolysis liquids derived from second-generation bioethanol production residues over NiMo and CoMo catalysts. Biomass and Bioenergy 2019;126:84–93. https://doi.org/https://doi.org/10.1016/j.biombioe.2019.05.005.

[26] Ardiyanti AR, Gutierrez A, Honkela ML, Krause AOI, Heeres HJ. Hydrotreatment of wood-based pyrolysis oil using zirconia-supported mono- and bimetallic (Pt, Pd, Rh) catalysts. Appl Catal A Gen 2011;407:56–66. https://doi.org/https://doi.org/10.1016/j.apcata.2011.08.024.

[27] Kloekhorst A, Wildschut J, Heeres HJ. Catalytic hydrotreatment of pyrolytic lignins to give alkylphenolics and aromatics using a supported Ru catalyst. Catal Sci Technol 2014;4:2367–77. https://doi.org/10.1039/C4CY00242C.

[28] Sahu R, Song BJ, Im JS, Jeon Y-P, Lee CW. A review of recent advances in catalytic hydrocracking of heavy residues. J Ind Eng Chem 2015;27:12–24. https://doi.org/https://doi.org/10.1016/j.jiec.2015.01.011.

[29] Ni X, Miao J, Lv R, Lin X. Quantitative 3D spatial characterization and flow simulation of coal macropores based on μCT technology. Fuel 2017;200:199–207. https://doi.org/https://doi.org/10.1016/j.fuel.2017.03.068.

[30] Nanduri A, Mills PL. Effect of catalyst shape and multicomponent diffusion flux models on intraparticle transport-kinetic interactions in the gas-phase Fischer-Tropsch synthesis. Fuel 2020;278:118117. https://doi.org/https://doi.org/10.1016/j.fuel.2020.118117.

[31] Reyes-Antonio CA, Cordero ME, Pérez-Pastenes H, Uribe S, Al-Dahhan M. Analysis of the effect of hydrodynamics over the activity and selectivity of the oxidative dehydrogenation of propane process in a packed bed reactor through

518 CFD techniques. Fuel 2020;280:118510.
519 https://doi.org/https://doi.org/10.1016/j.fuel.2020.118510.

520 [32] Soloveva O V., Solovev SA, Egorova SR, Lamberov AA, Antipin A V.,
521 Shamsutdinov E V. CFD modeling a fluidized bed large scale reactor with various
522 internal elements near the heated particles feeder. Chem Eng Res Des
523 2018;138:212–28. https://doi.org/10.1016/j.cherd.2018.08.011.

524 [33] Bathe K-J. Finite Element Procedures. 2nd ed. 2012.

525 [34] Mimura K, Oka D, Sato T, Itoh N. CFD Analysis of a Single Palladium Membrane
526 Tube Reactor for the Dehydrogenation of Cyclohexane as a Chemical Hydrogen
527 Carrier. vol. 43. 2010. https://doi.org/10.1252/jcej.09we207.

528 [35] Mimura K, Yoshida N, Sato T, Itoh N. CFD Analysis and Design of Multi-tubular
529 Membrane Reactor for Dehydrogenation of Cyclohexane. vol. 53. 2010.
530 https://doi.org/10.1627/jpi.53.283.

531 [36] Byron Smith RJ, Muruganandam L, Murthy Shekhar S. CFD analysis of water gas
532 shift membrane reactor. Chem Eng Res Des 2011;89:2448–56.
533 https://doi.org/http://dx.doi.org/10.1016/j.cherd.2011.02.031.

534 [37] Said SAM, Simakov DSA, Mokheimer EMA, Habib MA, Ahmed S, Waseeuddin
535 M, et al. Computational fluid dynamics study of hydrogen generation by low
536 temperature methane reforming in a membrane reactor. Int J Hydrogen Energy
537 2015;40:3158–69.
538 https://doi.org/http://dx.doi.org/10.1016/j.ijhydene.2015.01.024.

539 [38] Habib MA, Ahmed P, Ben-Mansour R, Badr HM, Kirchen P, Ghoniem AF.
540 Modeling of a combined ion transport and porous membrane reactor for oxy-
541 combustion. J Memb Sci 2013;446:230–43.

https://doi.org/http://dx.doi.org/10.1016/j.memsci.2013.06.035.

[39] Ahmed P, Habib MA, Ben-Mansour R, Kirchen P, Ghoniem AF. CFD (computational fluid dynamics) analysis of a novel reactor design using ion transport membranes for oxy-fuel combustion. Energy 2014;77:932–44. https://doi.org/http://dx.doi.org/10.1016/j.energy.2014.10.003.

[40] Roses L, Manzolini G, Campanari S. CFD simulation of Pd-based membrane reformer when thermally coupled within a fuel cell micro-CHP system. Int J Hydrogen Energy 2010;35:12668–79. https://doi.org/http://dx.doi.org/10.1016/j.ijhydene.2010.07.080.

[41] Marchisio DL, Rivautella L, Barresi AA. Design and scale-up of chemical reactors for nanoparticle precipitation. AIChE J 2006;52:1877–87. https://doi.org/10.1002/aic.10786.

[42] España G de. Real Decreto 61/2006 de 31 de enero de 2006, por el que se determinan las especificaciones de gasolinas, gasóleos, fuelóleos y gases licuados del petróleo y se regula el uso de determinados biocarburantes. BOE – A – 2006 – 2779 2006;Real Decre.

[43] International A. Standard Test Method for Density, Relative Density, and API Gravity of Liquids by Digital Density Meter 2018;D4052 – 18. https://doi.org/https://doi.org/10.1520/D4052-18A.

[44] International A. Standard Test Methods for Flash Point by Pensky-Martens Closed Cup Tester 2018;D93 – 18. https://doi.org/https://doi.org/10.1520/D0093-18.

[45] (CEN) EC for S. Automotive fuels - Fatty acid methyl ester (FAME) fuel and blends with diesel fuel - Determination of oxidation stability by accelerated oxidation method 2014;EN 15751:2.

[46] (CEN) EC for S. Petroleum products. Determination of sulfur content of automotive fuels. Ultraviolet fluorescence method. 2011;EN 20846:2.

[47] International A. Standard Test Method for Bromine Numbers of Petroleum Distillates and Commercial Aliphatic Olefins by Electrometric Titration 2017;D1159 – 07.

[48] Escola JM, Aguado J, Serrano DP, Briones L. Transportation fuel production by combination of LDPE thermal cracking and catalytic hydroreforming. Waste Manag 2014;34:2176–84. https://doi.org/https://doi.org/10.1016/j.wasman.2014.06.010.

[49] Donald A. Nield AB. Convection in Porous Media. Third Edition. United States of America: Springer; 2006.

[50] Matyka M, Khalili A, Koza Z. Tortuosity-porosity relation in porous media flow. Phys Rev E 2008;78:26306.

[51] Pisani L. Simple Expression for the Tortuosity of Porous Media. Transp Porous Media 2011;88:193–203. https://doi.org/10.1007/s11242-011-9734-9.

[52] Bruce E. Poling John O' Connell JMP. The properties of gases and liquids. 5th edition. New York, Chicago, San Francisco, Athens, London, Madrid, Mexico City, Milan, New Delhi, Singapore, Sydney, Toronto: McGraw-Hill Education; 2000.

[53] Fan Y, Yin J, Shi G, Liu H, Gao J, Bao X. A Six-Lump Kinetic Model for Olefin Hydrogenation, Hydroisomerization and Aromatization in FCC Gasoline Hydro-Upgrading. Catal Letters 2009;129:181–8. https://doi.org/10.1007/s10562-008-9788-7.

[54] Richardson SM, Gray MR. Enhancement of residue hydroprocessing catalysts by

doping with alkali metals. Energy and Fuels 1997;11:1119–26. https://doi.org/10.1021/ef970001l.

[55] Lu WZ, Teng LH, Xiao W De. Simulation and experiment study of dimethyl ether synthesis from syngas in a fluidized-bed reactor. Chem. Eng. Sci., vol. 59, Pergamon; 2004, p. 5455–64. https://doi.org/10.1016/j.ces.2004.07.031.

[56] Arab S, Commenge JM, Portha JF, Falk L. Methanol synthesis from CO2 and H2 in multi-tubular fixed-bed reactor and multi-tubular reactor filled with monoliths. Chem Eng Res Des 2014;92:2598–608. https://doi.org/10.1016/j.cherd.2014.03.009.

[57] Speight JG. Fouling During Hydrotreating. Fouling in Refineries, Elsevier; 2015, p. 303–28. https://doi.org/10.1016/b978-0-12-800777-8.00012-7.

[58] AspenTech, editor. Aspen Plus v10 2017.

[59] Aspen Technology I. Aspen Physical Property System. Physical Property Models. 2010.

[60] Chen X, Yang L, Dai H, Shi S. Exploring factors controlling pre-corrosion fatigue of 316L austenitic stainless steel in hydrofluoric acid. Eng Fail Anal 2020;113:104556. https://doi.org/https://doi.org/10.1016/j.engfailanal.2020.104556.